AD_____
(Leave blank)

Award Number: W81XWH-07-2-0085

TITLE: Improving Soldier Recovery from Catastrophic Bone Injuries: Developing a*n animal model for standarizing the bone reparative potential of emerging progenitor cell therapies*

PRINCIPAL INVESTIGATOR:

David W. Rowe, M.D. (PI)   Liisa Kuhn, Ph.D. (associate)
Douglas Adams, Ph.D. (CoPI)   Mei Wei, Ph.D. (associate)
Dong-Guk Shin, Ph.D. (CoPI)   Jay Lieberman, M.D. (associate)

CONTRACTING ORGANIZATION: University of Connecticut Health Center
                          Farmington, CT 06030

REPORT DATE: August 2008

TYPE OF REPORT: Annual

PREPARED FOR: U.S. Army Medical Research and Materiel Command
              Fort Detrick, Maryland 21702-5012

DISTRIBUTION STATEMENT: (Check one)

   x Approved for public release; distribution unlimited

     Distribution limited to U.S. Government agencies only; report contains proprietary information.

REPORT DOCUMENTATION PAGE

Form Approved
OMB No. 0704-0188

1. REPORT DATE *(DD-MM-YYYY)* 31-08-2008	2. REPORT TYPE Annual	3. DATES COVERED *(From - To)* 1 AUG 2007 - 31 JUL 2008

4. TITLE AND SUBTITLE Improving SolRecovery from Catastrophic Bone Injuries: Developing *an animal model for standardizing the bone reparative potential of emerging progenitor cell therapies*	5a. CONTRACT NUMBER W81XWH-07-2-0085
	5b. GRANT NUMBER
	5c. PROGRAM ELEMENT NUMBER
6. AUTHOR(S) David W. Rowe, M.D. Email: rowe@neuronuchcedu	5d. PROJECT NUMBER
	5e. TASK NUMBER
	5f. WORK UNIT NUMBER

7. PERFORMING ORGANIZATION NAME(S) AND ADDRESS(ES) University of Connecticut Health Center Farmington, CT 06030	8. PERFORMING ORGANIZATION REPORT NUMBER

9. SPONSORING / MONITORING AGENCY NAME(S) AND ADDRESS(ES) U.S. Army Medical Research and Materiel Command Fort Detrick, Maryland 21702-5012	10. SPONSOR/MONITOR'S ACRONYM(S)
	11. SPONSOR/MONITOR'S REPORT NUMBER(S)

12. DISTRIBUTION / AVAILABILITY STATEMENT
Approved for public release; distribution unlimited

13. SUPPLEMENTARY NOTES

14. ABSTRACT

During the first year of this award, we have demonstrated that mice carrying transgenic GFP reporters that reflect the level of osteoblast differentiation and the host/donor origin of these cells provides a rapid, highly informative and ultimately quantitative interpretation of a transplantation experiment of skeletal stem cells into a critical size bone defect. The calvarial defect model has been the primary platform to test a number of donor cell preparations and scaffold formulations. A combination of neonatal calvarial progenitors and a commercial scaffold achieves complete healing of the lesion occurs within in 3-4 months. Using this combination as a reference standard, we have begun to examine clinically relevant tissue sources and scaffolds with improved biomechanical properties that would be more appropriate for a long bone defect. To better understand the cellular basis of a long bone defect, we have utilized the GFP reporters in the closed tibial fracture. The surprise finding is the extent of activity of early vascular and skeletal progenitors that initiates well away from the fracture site and grows forward to form the callus. In the coming year we will apply the information learned from the calvarial defect to a non-union extension of the tibial fracture model.

15. SUBJECT TERMS
None provided.

16. SECURITY CLASSIFICATION OF: U			17. LIMITATION OF ABSTRACT	18. NUMBER OF PAGES	19a. NAME OF RESPONSIBLE PERSON USAMRMC
a. REPORT U	b. ABSTRACT U	c. THIS PAGE U	UU	22	19b. TELEPHONE NUMBER *(include area code)*

Standard Form 298 (Rev. 8-98)
Prescribed by ANSI Std. Z39.18

Table of Contents

INTRODUCTION

This proposal was developed to face the reality that the most optimal scaffold, cell source and host preparation for repair of a critical sized skeletal defect is yet to defined. Furthermore the best combination of these factors is likely to be identified in a trial and error approach. This is unlikely to be hypothesis driven research nor is it a process that can be adequately explored in traditional large animal models. We want to demonstrate that a fast, informative, quantitative and biologically relevant process to initially screen for the most promising candidate factors can be developed using a series of GFP-reporter mice and bone repair models. As the best candidates are identified, they will be evaluated in an increasingly more demanding repair setting so that at the end of the process a rational process can select the protocols most deserving of evaluation in a large animal model. An even longer-range goal is to adapt the models and reporter systems so that human derived progenitor cells can be evaluated in the same high throughput system as the basis for eventual clinical trials. Our year 1 statement of work (SOM) as presented in the application is directed at establishing the models and beginning the evaluation of cell sources and scaffolds.

- *Transplantation of progenitor cells (bone, capillary and blood vessels) from bone out-growth cells, bone marrow stroma, adipocyte stroma, fetal cord cells and murine ES cells will be evaluated in models 1 and 2. In most cases the cells will be isolated and expanded in culture under condition that promote expansion of the desired progenitor cell as indicated in the transplantation models.*
- *Begin the evaluation of various scaffolds for introducing progenitor cells into the calvarial defect model (3). Develop the in vivo evaluation of the repair using our new in vivo analysis facility.*
- *Begin work on the extremity defect model by first defining fracture repair using the GFP reporter mice. As the fracture severity is increased, implement the segmental defect model using external fixators.*

Not included in the SOM was the plan for developing image analysis to the evaluation of a bone repair experiment nor was it recognized that a database to organize and retrieve the numerous images that are inherent in a repair experiment would need to be developed.

It was a very productive first year and this report is organized to reflect the major topical issues as objectives. The report will illustrate some of the histological features that support the interpretation provided within the text, but the images are not comprehensive.   The report should help to focus the questions and issues that will be the subject of the site visit team scheduled for September 25, 2008.

BODY

Objective 1: Transplantation model.

We initially proposed the intra marrow (model 1) and heterotopic bone (model 2) transplantation model to evaluate various sources for adult progenitor cells. However as we became familiar with the calvarial defect model (3) it became clear that is was far superior assessing progenitor source as well as scaffold design. Therefore we have abandoned models 1 and 2 and have focused and expanded the utility of the model 3. Dr. Liping Wang, now a senior research associate in the Rowe laboratory, has performed the majority of the calvarial defect work.

A. Progress over the past year
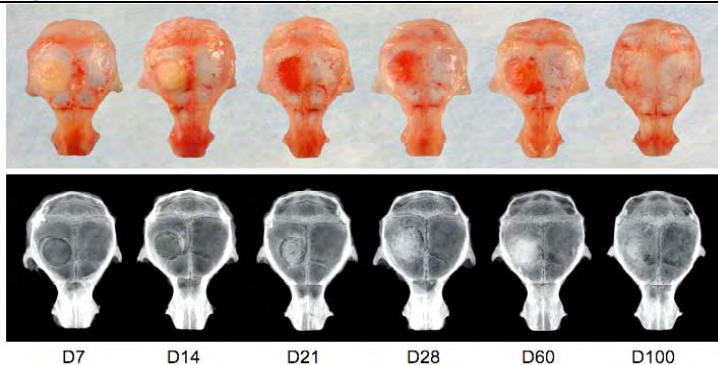
Figure 1: The photographic and X-ray appearance of a single calvarial defect filled with a hydroxyapatite-based scaffold containing neonatal calvarial bone progenitor cells. Intense vascularity is associated with new bone formation starting by day 21. Between day 60 and 100 the newly made bone remodels and integrates with the surrounding bone. This progression will be analyzed separately as early and late bone formation.

D7   D14   D21   D28   D60   D100

1. **Single hole calvarial defect model**: We initially followed the literature suggesting that a 4-5 mm hole created in the frontal/parietal bone will not self heal and that the mice can tolerate this surgery and function normally for at least 60 days without intervention. Using commercially available scaffolds and neonatal calvarial cells as our best bone progenitor source ($5x10^5$), we were able to demonstrate complete healing of the defect over a 3-4 month process. Figure 1 shows the sequence of gross morphological events and the intense vascularity that accompanies the new bone formation and it subsequent remodeling into the adjacent bone. Even from the gross appearance, the process can be conceptualized as a continuum of three stages: preossification, active ossification and remodeling/integration. Eventually we need to understand the cellular basis of each stage. The following illustrates our progress in defining the cellular events.

a. *Although the host does contribute cells to the critical size defect, these cells do not differentiate into osteoblasts.* Host mice carrying the Col3.6GFPtpz (green) reporter that had the calvarial defect filled with either Gelfoam or Helos only (no donor cells). The defect was examined at 28 and 60 days; no bone was formed confirming the model is a critical size. Figure 2 shows the cellular response within the host bone and defect zone. The bright green line of cells overlying a red label are host osteoblasts
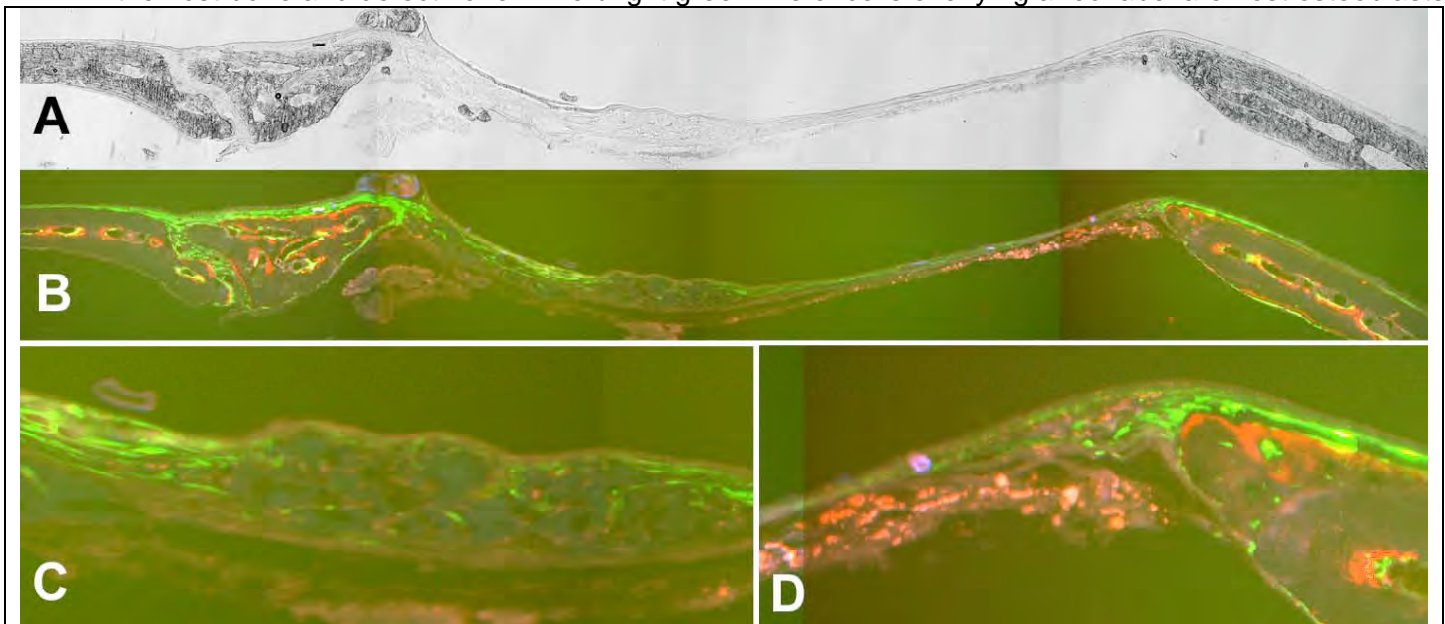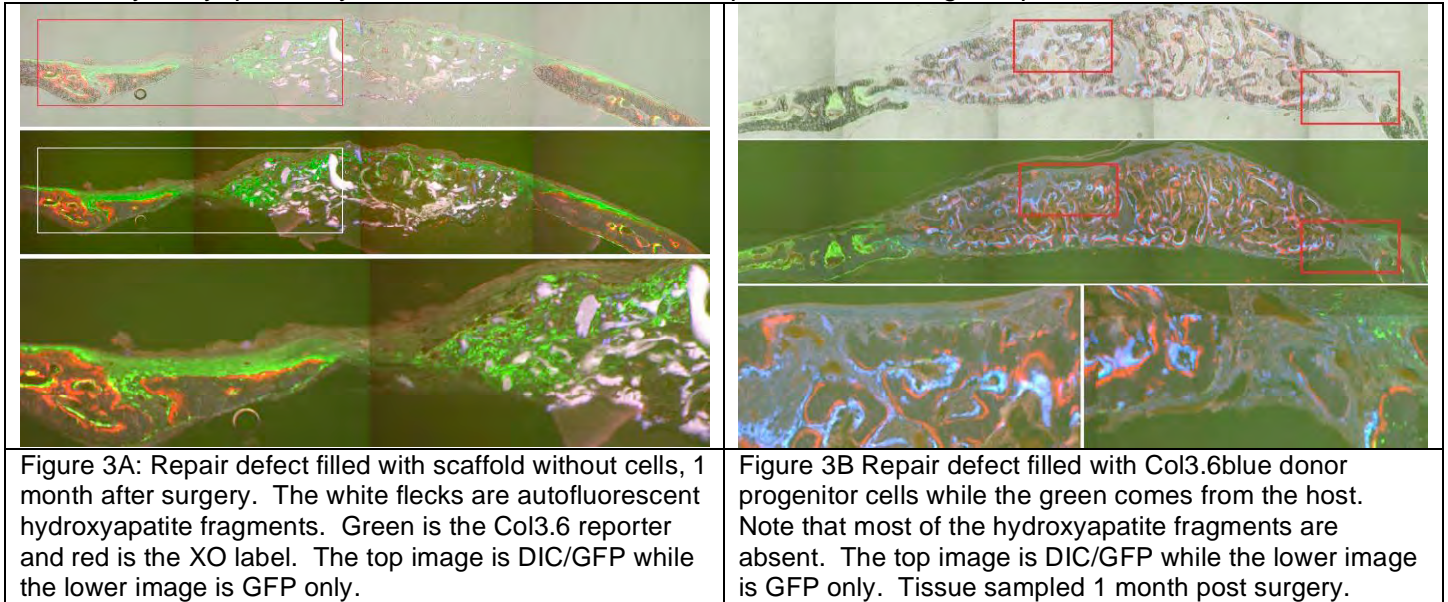

Figure 2: A 4 mm calvarial defect repair 28 days after a repair with gel foam scaffold only. A. DIC and B-D are overlays of the blue, green and red filters. Fibroblastic cells extend from the host into lesion but these cells do not differentiation into osteoblasts. Panel D shows host osteoblasts in the peripheral bone.

within the surrounding bone lying down newly mineralizing bone which is stained red because the mice had been injected with xylenol orange (XO) one day prior to sacrifice. Green cells that are more fibroblastic in appearance but less bright than the osteoblasts appear to be streaming out from the central suture towards the defect zone. The cell that reach the repair zone gradually fill the space but none of these cell acquire the rounded shave/high intensity of an osteoblast nor is there deposition of the XO label. For these cells to differentiate will probably require the scaffold to provide one or more growth/differentiation factors, a topic that we currently are not exploring.

b. *Donor derived progenitors from neonatal calvaria account for the vast majority of bone made in the calvarial defect model.* Figure 3 illustrates the outcome of bone formed when the scaffold (Helos) is inoculated with donor cells derived from a Col3.6blue donor. Without inoculation (3A), the Helos persists in the defect area but is invested by donor cell. Similar to gelfoam, the host cells are fibroblasts and fail to acquire the GFP characteristic of an osteoblast even thought these is intense osteogenesis in the surrounding host bone. Helos is a collagen fiber, hydroxyapatite composite that has sufficient structure to make inoculation with donor cells fairly reproducible. The hydroxyapatite is autofluorescent and partially opaque to X-ray and μCT. However it is readily distinguished from new bone formation because it does not label with XO and is not associated with GFP+ osteoblasts. An interesting property of the material is that the hydroxyapatite crystals remain stable when no bone is made, but is rapidly removed in association with new bone formation. The bone that is formed (figure 3B), as seen by DIC optics and by fluorescent imaging, has the red XO label on its surface and strong blue osteoblasts above the label line. There is very little contribution of host green cells within the bone

and those cells which are on the bone surface have proven to be donor-derived osteoclasts (shown later). One interpretation of the outcome is that most of the bone forming activity has been provided by the donor cells and in some manner the signal for host participation is restricted. Note that the hydroxyapatite crystals have been resorbed as part of the osteogenic process.

Figure 3A: Repair defect filled with scaffold without cells, 1 month after surgery. The white flecks are autofluorescent hydroxyapatite fragments. Green is the Col3.6 reporter and red is the XO label. The top image is DIC/GFP while the lower image is GFP only.

Figure 3B Repair defect filled with Col3.6blue donor progenitor cells while the green comes from the host. Note that most of the hydroxyapatite fragments are absent. The top image is DIC/GFP while the lower image is GFP only. Tissue sampled 1 month post surgery.

b. *Donor derived bone is remodeled toward a membranous bone composed of mature osteoblasts and osteocytes with significant input from host osteoclasts.* Figure 4 shown the 60-day time point of Col3.6blue donor cells inoculated into the lesion in a Col3.6green host animal. The histological pattern is more complex The reduced number of strong blue osteoblast overlying an red XO label is consistent with the behavior of the Col3.6 promoter which is active in early osteoblasts but is lost from more
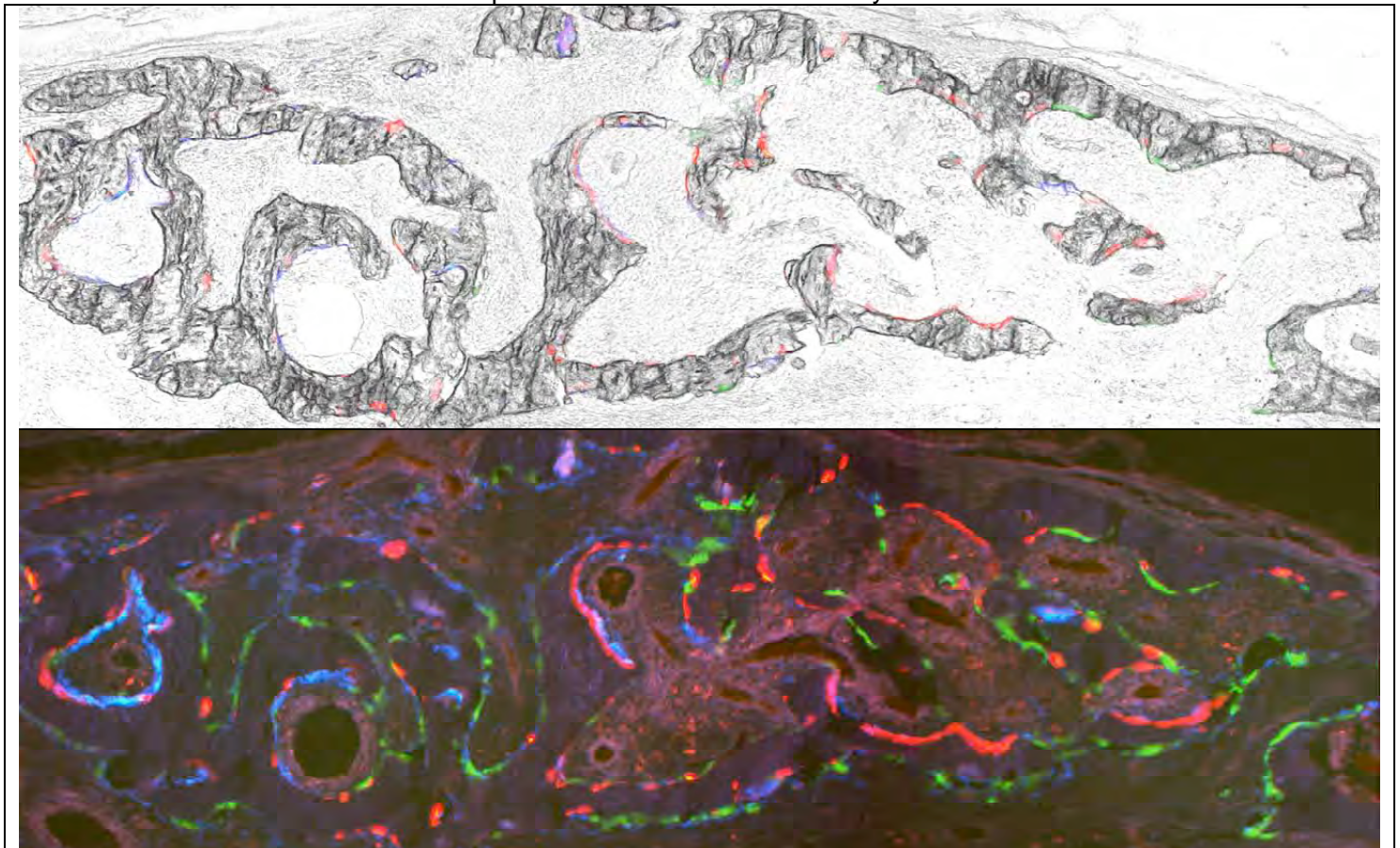

Figure 4: Day 60 repair of gelfoam scaffold seeded with Col3.6GFPcyan calvarial donor cells. The upper panel is the DIC image and the lower has the DIC removed. Note the fibrous nature of the tissue between the bone.

mature cells and osteocytes. More prominent are the green bone lining cells that are not overlying a XO red label. These have proven to be host derived myeloid cells (1,2), most of which are TRAP positive indicating that they are of the osteoclast lineage (figure 5). At the periphery of the repair, there can be suggestion of intermingling of blue and green osteoblast which we believe will be the hallmark of integration of host and donor bone. The host bone cells are recognized by their stronger expression and association with the red label. Also note that the fibrous nature of the tissue between the bone indicating that bone marrow is not well developed when calvarial donor cells are used.
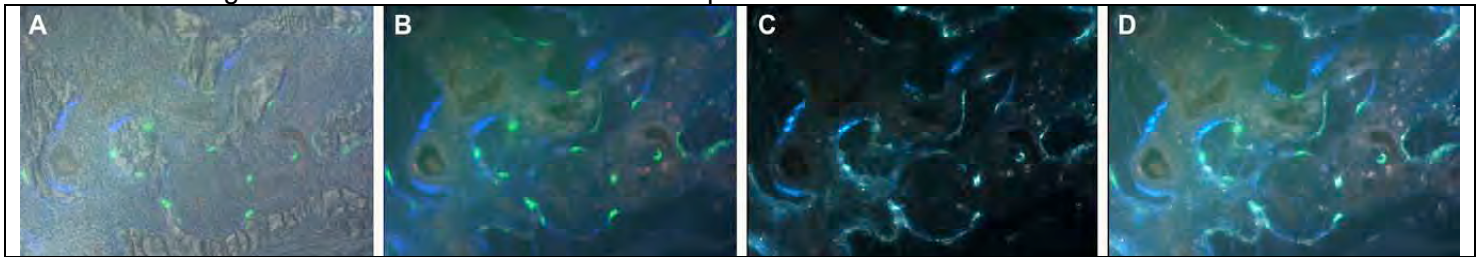

Figure 5: The green bone lining cells are not osteoblasts. A section from figure 4 that was stained for TRAP using a fluorescent substrate. A. The DIC overlay image in which the XO label is lost during the acidic conditions of the TRAP stain. B. The DIC removed to reveal the blue and green bone lining cells. C. The TRAP stain using a filter that does not totally exclude the blue or green of B. Note that the white fluorescence comes from the green cells. D. Overlay of B and C.

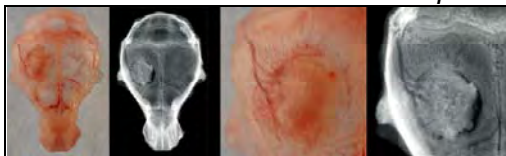c. *Vasculature within the repair zone come from host* – During the phase of rapid new bone formation, the repair zone is extremely vascular and large blood vessels feeding the repair zone develop from the host bone (Figure 6). Clearly understanding the cellular origins of the vascular system will be important to the ultimate repair strategy. Figure 7 illustrates the repair zone of mice bearing complementary colors of SMAA-GFP reporter which is weakly active in the myofibroblast that will progress to a Col3.6 positive cell and is particularly strong in the smooth muscle layer of small arteries and arterioles (3). By transplanting SMAA red into a host that is SMAA green, the contribution of either cell source can be appreciated. The figure legend describes the details that suggest that the donor cells that will form bone go through a SMAA stage while the blood vessels that support the growth of the donor cells come from the host. This is a very preliminary result that indicates that the inoculating cells are not uniformly distributed but instead accumulate at the base of the scaffold.

Fig 6: Large vessels supply the bone that develops within the repair zone. Left pair is Helos alone, and right pair is inoculated scaffold.
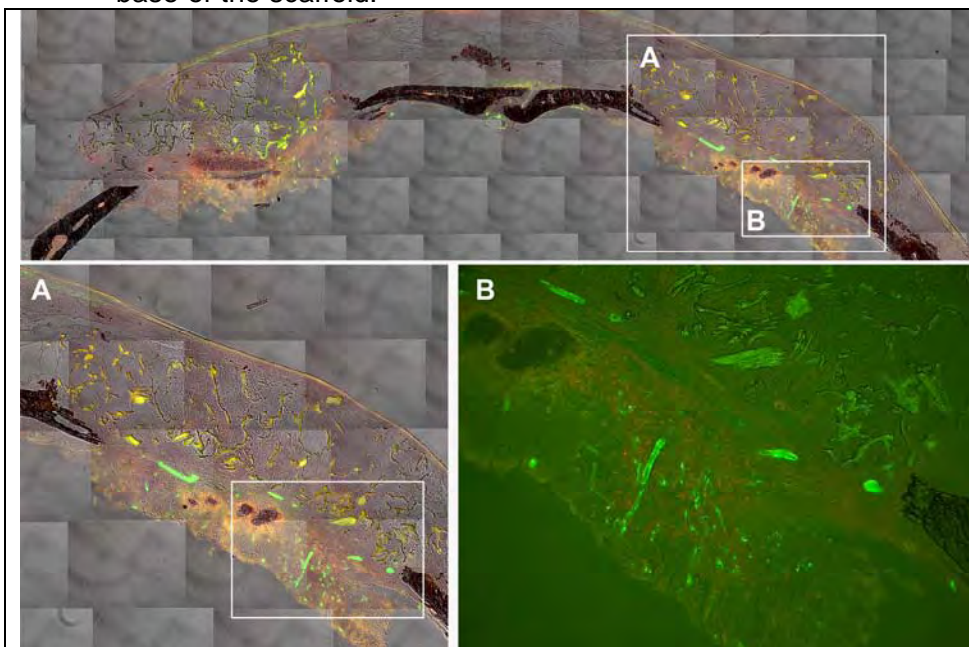
Figure 7: Day 7 after transplantation of SMAA-red into a SMAA-green host using Helos as the scaffold. Top panel shows where the detailed histology of panel B is taken. Panel B shows red fibroblastic like cells that appear to be at the base of the scaffold that are adjacent to tubular green structures (muscular vessels). Although myofibroblastic like green cells are also present, they do not appear to intermingle with the red cells. The left defect received calvarial cells only, while the right defect received calvarial and fresh bone marrow cells. Future experiments will mix osteogenic progenitors with endothelial progenitors .

d. *Freshly harvested marrow does not contribute to new bone formation -* Reports in the literature still conclude that freshly harvested marrow or the non-adherent cell population of a marrow culture are highly osteogenic (4, 5). Although we published previously that this a misinterpretation of their data

(the bone lining cells are myeloid not osteogenic), those experiments utilized intramarrow transplantation (1,2). We wanted to repeat the experiments using the calvarial defect model. When the source of donor cell inoculated into the scaffold was marrow only (either fresh or non-adherent), no bone was formed and the histology resembled the images of non-inoculated scaffold (see fig 11). One explanation for the success of marrow might be a contribution of bone progenitors attached to bone fragments. The fragments or the early progenitors that arise from the fragments might influence bone marrow cells to become osteogenic (6). To test this possibility, calvarial progenitors from a Col3.6blue donor were mixed with freshly isolated marrow from a Col3.6green donor prior to inoculation into a scaffold and implanted in a non-transgenic host. At 4 and 8 weeks bone was formed, but the osteogenic portion was provided by blue osteoblasts. Again, green bone lining cells were present, but they did not overly an XO label and they are TRAP positive. It is our subjective observation that the repair zone may have remodeled more rapidly when the marrow cell were present, but this impression needs to be tested in a more objective manner.

e. *Adherent bone marrow cells are osteogenic, although not to the degree as calvarial progenitors* – The cells that attach to plastic and begin to form clusters of cell that eventually will make a mineralized nodule go through a transition of GFP expression that is SMAA->Col3.6weak->Col3.6strong->Col2.3/osteocalcin. Harvesting a culture between days 4-7 enriches for the SMAA/Col3.6weak population. However when compared to a equal number of calvarial progenitor cells, the amount of resulting bone is significantly less in either the intramarrow transplantation of calvarial defect model (not show directly, but see figure 11).

Figure 8: Bone formation by DermoCre/ZEG cells expanded as a micromass culture. Panel A shows bone formation by xray and XO fluorescence using the IVIS imaging system. Note that the GFP- population produces a hyperemic repair zone, but is does not lead to osteoganesis; Panel B is a histological section through the repair region. Arrows show XO staining and the resorption of the hydroxyapatite crystals associated with bone formation.

On going experiments from one of my NIH grants is trying to identify earlier reporters for the osteogenic lineage. Using a Dermo1-cre promoter driving a floxed GFP reporter, a population of just recombined progenitors can be identified and isolated by FAC sorting from a day 2-3 stromal cell culture and then replated as a microdot of cells. These cells expand in number at an extremely rapid rate and can be induce to osteogenesis. However if these expanding cells are inoculated into a scaffold, bone is vigorously made that exceeds our calvarial standard (figure 8). Because the experimental design used a lineage reporter, the GFP that is present in the lesion does not reflect the level of osteogenic differentiation. This experimental protocol will be applied to our differentiation sensitive reporter mice to better understand the cell population that expands and retains its strong

osteogenic capability.   The experiment also underlines the need to developing a way to demonstrate the enrichment for progenitor cells from various sources for bone repair.

2. **Double hole calvarial defect model** – As we gained experience with the one-hole calvarial model, some of its drawback became more evident, chief among them was the lack of a control or reference lesion in the same animal. A two hole model could provide a control/reference in the same animal further increasing the through put and quantitative aspects of our transplantation model. We obtained permission to modify our animal care protocol to place two 3.5 mm hole on either side of the frontal/parietal bones. This protocol is as well tolerated as the single hole and 3.5 mm does not heal spontaneously. Figure 9 shows the progression of healing using this model which temporally is similar to the one hole model. Helos has become our default
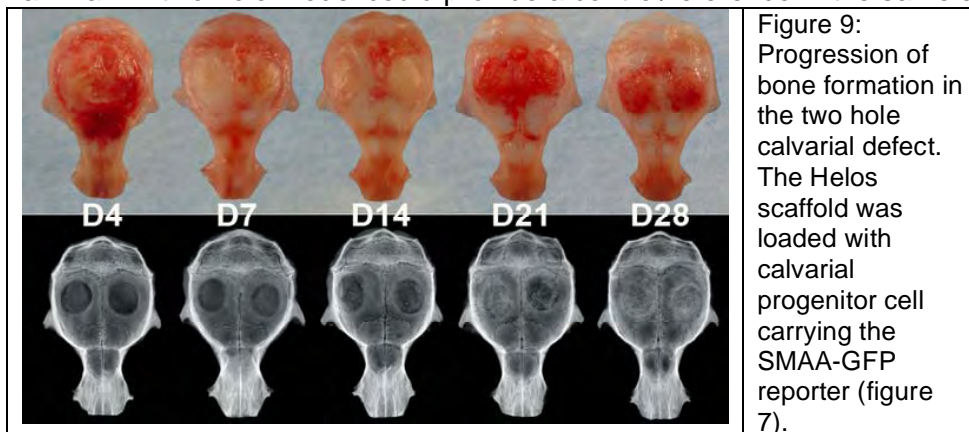

Figure 9: Progression of bone formation in the two hole calvarial defect. The Helos scaffold was loaded with calvarial progenitor cell carrying the SMAA-GFP reporter (figure 7).

standard (reference) scaffold and neonatal calvarial progenitors is the standard progenitor source – Helos is a collagen fiber, hydroxylapatite composite that has sufficient structure to make inoculation with donor cells fairly reproducible. The hydroxylapatite is autofluorescent and partially opaque to X-ray and µCT. However it is readily distinguished from new bone formation because it does not label with XO and is not associated with GFP+ osteoblasts. An interesting property of the material is that the hydroxyapatite crystals remain stable when no bone is made, but is rapidly removed in association with new bone formation.

  a. *Helos is superior to scaffold A* – Dr. Kuhn arranged to have an experimental scaffold (A) provided by a prominent material science group to be tested in the two hole model. The host was Col3.6green and the donor is Col3.6blue from neonatal calvaria. Scaffold A has an autofluorescent background although it does not appear opaque to X-ray. Figure 10 shows the quantification of bone formation by µCT.
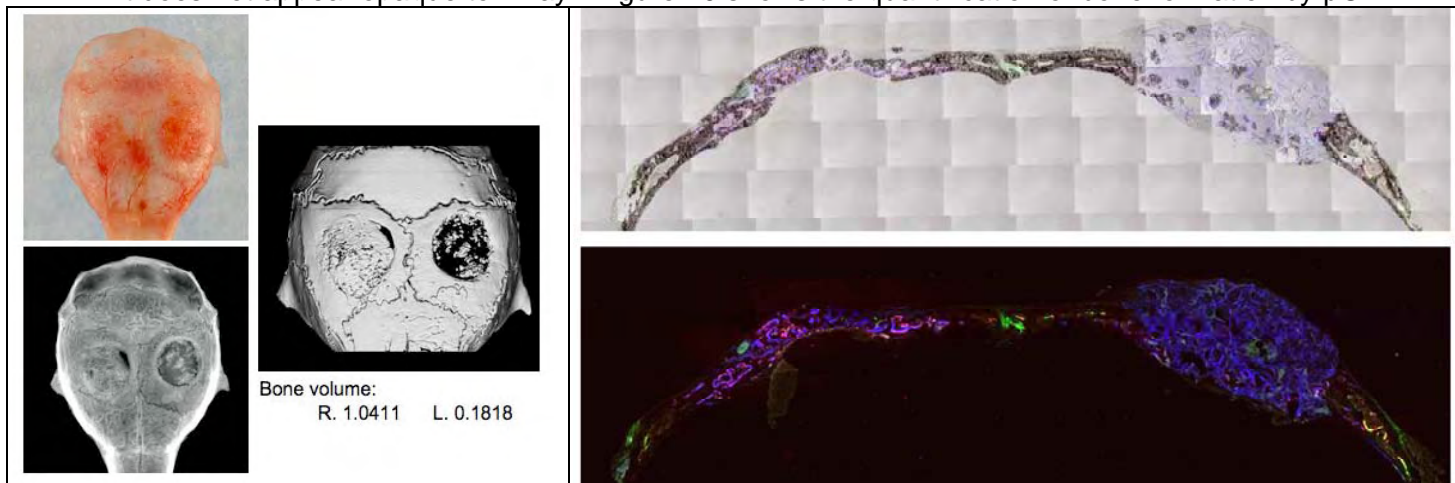

Bone volume:
R. 1.0411   L. 0.1818

Fig 10: The two hole calvarial model used to contract two different scaffold types for bone repair when seeded with neonatal osteoprogenitor cells. This is a 60 day sample in which the control repair show extensive remodeling toward compact bone and a reduction of vascularity, while the test material shows good vascularity but only scattered islands of bone and little evidence of scaffold resorption. High power analysis (not shown) reveals that fibroblastic like cells persist in the test repair area indicating that the material did not support osteoblast differentiation.

The histology demonstrates new bone formation in the Helos side (blue cells with red mineralization line) while the scaffold A is blue without the red line. Scaffold A remains unresorbed with bone formation (host and donor origin) limited to sites adjacent to host bone. Another set of test scaffolds supplied by Dr. Mei Wei is currently undergoing testing to further refine our analytical model. Some of here samples have a composition that resembles Helos so we anticipate better osteogenic differentiation. One advantage of the scaffolds that she is producing is the potential for adding exogenous growth factors that potentially could induce more host participation in the repair.

b. Comparison of tissue sources of bone progenitors – Preliminary experiments appear to indicate that adipocyte stromal cells are not a good source of progenitors at least as currently grown and harvested. Whether implanted in Helos or scaffold A, little osteogenesis is observed and most donor derived osteoblasts occurred at the interface of host bone. Cells do survive and populate the scaffolds but do not progress to osteogenesis (data not shown). We have also found the fetal cord blood, fetal cord fibroblasts and placental fibroblast fail to generate bone in the intramarrow transplantation model. While this was not surprising, the failure of adipocyte stromal cells was a disappointment that we need to explore further because it is an accessible source of progenitors.

Another experiment contrasted marrow adherent stromal cells to freshly isolated bone marrow cells. As expected no bone formed from the fresh marrow source. However the extent of bone that resulted from the marrow adherent cells was quite variable. The best sample formed what appears to be cortical bone with extensive marrow elements, much different from the bone formed by calvarial progenitors. There experiment need repeating and at best have to be considered preliminary, but do suggest that the type of progenitor used for a membranous bone defect may be different than that used for a long bone defect.
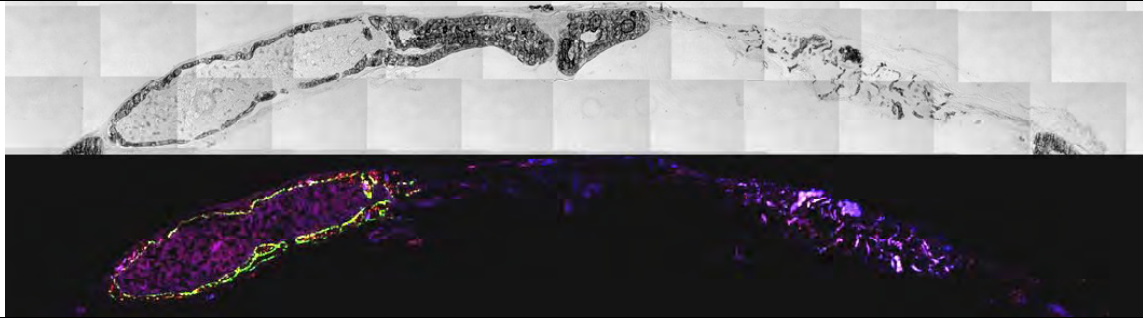

Figure 11: Bone formed in Helos scaffold from marrow adherent cells (unenriched). The donor is a double transgenic donor (BSP/DMP1) that marks more mature cells. Although there was significant variability for bone formation on the left side inoculated by the adherent cells, no bone formation was ever seen on the right side which was filled with non-adherant bone marrow cells. Note that the character of the bone formed on the left side is not woven/membranous as is the case with calvarial progenitors. This finding my have bearing on the source of donor cells used for the long bone defect model.

B. Plans for the coming year

We will focus on making the two hole calvarial model the most efficient and effective platform to evaluate progenitors and scaffolds. Already modification have been made in the way the calvarial tissue is processed for sectioning and imaging that will reduce the time required to acquire images for analysis. The analytical process will also be streamlined (see objective 3A). Using this two hole model we will complete our survey of viable tissue sources for osteogenic progenitors (adipose stroma, long bone outgrowth cells and marrow stromal cells as part of our funded NIH grant on adult stem cells) and work extensively with the scaffolds that are being produced by Dr. Wei and Kuhn. We also need to complete the analysis of endothelial and blood vessel investment of the healing wound and determine if donor endothelial and vascular cells can contribute to the repair process.

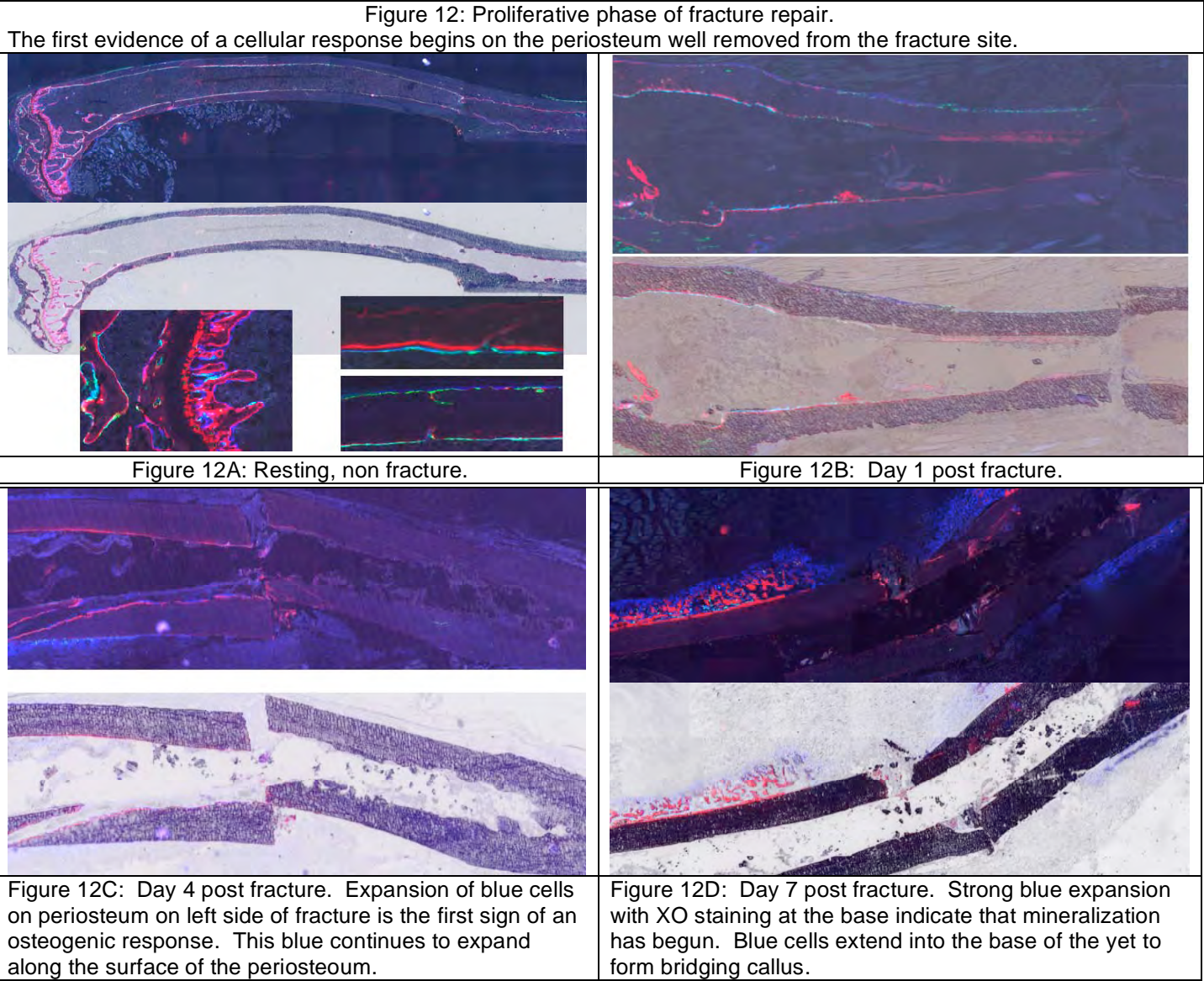## *Objective 2A: Establish the long bone fracture/repair model*
A. Progress over the past year

To better understand the cellular activities that are required for normal fracture healing and eventually to map the cellular basis of nonunion, we have initiated a comprehensive examination of the tibial fracture model in mice bearing GFP reporters of lineage progression. This project has been assumed by an orthopedic research fellow, Dr. Chikara Ushiku, with initial help in establishing the model from Dr. Douglas Adams. Dr. Ushiku has mastered the histological techniques and is currently adapting fluorescent in situ hybridization to map expression of crucial growth factors back to the GFP marked cells.

Three phases of fracture repair can be segmented by the GFP reporter mice. This was evident in the first experiments that we performed in a mouse transgenic for Col3.6blue (preosteoblasts and early osteoblasts) and hOCgreen (mature osteoblasts) that were injected with XO one day prior to sacrifice to label newly deposited bone mineral.

At base line, the expression of blue and green cells and XO bone is limited to the remaining primary metaphysis and surrounding cortical bone. Low level OC activity (green) without XO staining is present in the

endosteal cells of the diaphysis. One day after the fracture there appears to be XO staining of the endosteum near the fracture site with a noticeable lack of any GFP activity. Perhaps this represents loss of lining cells and exposure of mineralized surfaces to the XO label. Relative to later day, the periosteal layer appears to be inactive. The first sign of a GFP response was apparent at 3 days post fracture when weak Col3.6blue activity developed on the perisoteal surface well removed from the fracture site. These cells are not yet staining with XO suggesting that they are not yet making a mineralized matrix. By 5 days the blue cells had progressed toward the fracture site at what would become the base of the fracture callus. The lighter blue is present within the fracture space are likely to be a mixture of preosteoblasts and myofibroblasts that are better identified by another GFP marker (see methods). XO still labels bone surfaces lacking a GFP signal in the endosteal region near the fracture site. By day 7 the strong blue signal now is associated with strong XO labeling showing the wave on differentiation osteoblasts approaching the fracture site and followed by new mineralized matrix formation.

| Figure 12: Proliferative phase of fracture repair. |
| The first evidence of a cellular response begins on the periosteum well removed from the fracture site. |

| Figure 12A: Resting, non fracture. | Figure 12B: Day 1 post fracture. |

| Figure 12C: Day 4 post fracture. Expansion of blue cells on periosteum on left side of fracture is the first sign of an osteogenic response. This blue continues to expand along the surface of the periosteoum. | Figure 12D: Day 7 post fracture. Strong blue expansion with XO staining at the base indicate that mineralization has begun. Blue cells extend into the base of the yet to form bridging callus. |

The callus formation phase is well developed by day 11-14 (Figure 13). Strong blue cells now bridge the fracture and mineralization has begun (Figure 13A). At the base of the bridge, OC-green/Col3.6blue cells have appeared that extend into the bridging region by day 11. The dark areas beneath the bridged region and within the endosteal area are chondrocytes (day 11) develop strong TRAP staining (not shown) in association with vascular invasion and replacement of new mineralized blue bone formation by day 14 (Figure 13B).
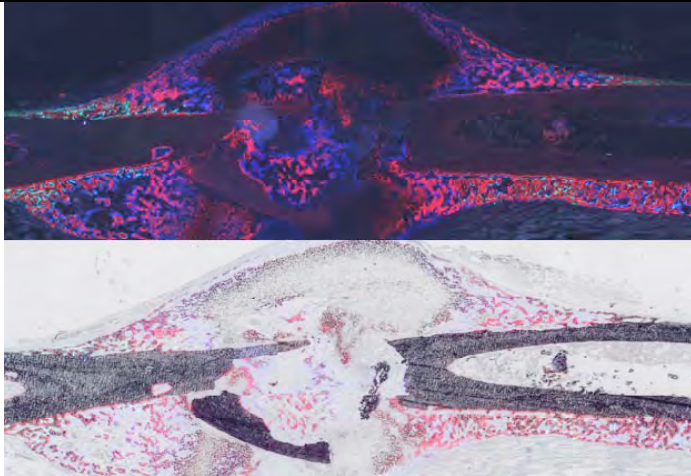
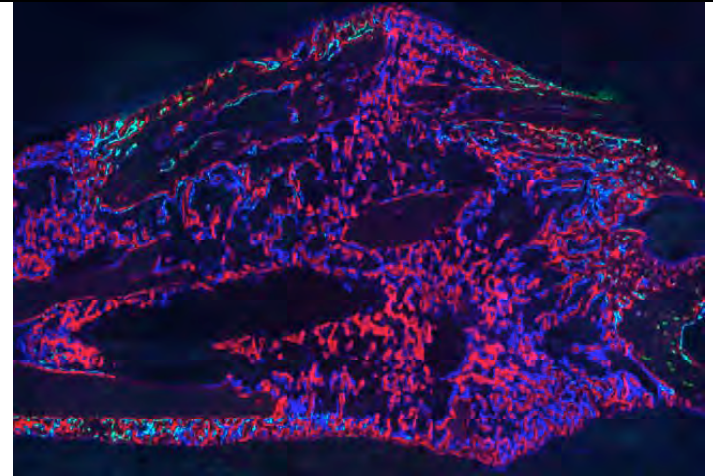| Figure 13: Bridging and callus formation	
Figure 13A: Day 11. Callus formation and bridging phase	Figure 13B: Day 14. Woven bone is replacing the cartilage.

By day 21 a residual area at the apex of the bridging region still have blue only cells associated with XO label. By 35 days the region is a mixture of blue/green cells that extends through the most of the bone even though it was not fractured. This is a remarkable extent of remodeling activity through out most of the cortical bone. At this point we do not know when the process is completed and the control state is regained.

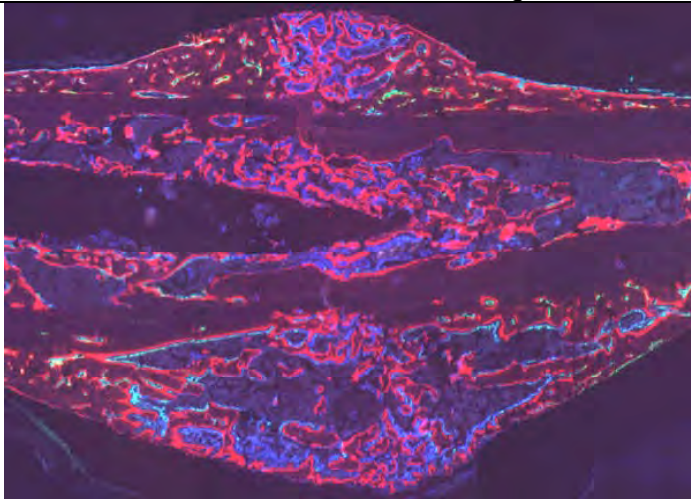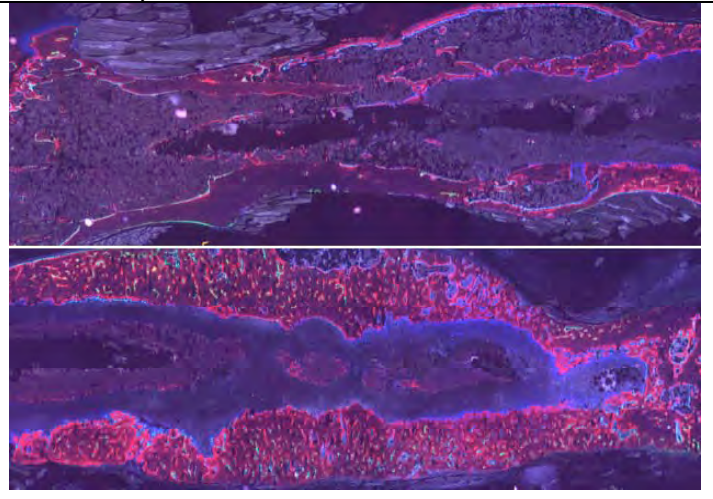| Figure 14: Callus resolution phase	
Figure 14A: Day 21. Maturation phase	Figure 14B: Day 35. Remodeling extends to host bone.

Based on this initial experience with the GFP reporters we are envisioning three phases of repair that will require a different set of reporters to fully appreciate: precallus; bridging and callus formation; callus resolution.

1. Precallus phase of fracture repair – This is likely the most important phase of the process because this is when the early progenitors for the vascular and skeletal elements proliferate. What was surprising was the distance away from the fracture site that the process initiates. To better appreciate the cellular basis of this early response, fractures were performed in SMAAgreen/Col3.6blue or Osterixgreen/Col3.6blue mice. The activity was examined at days 1,2 4 and 7 post fracture. The results of these studies is consistent with lineage progression of SMAA->Osterix->Col3.6weak->Col3.6strong (with XO staining).

Figure 15 illustrates the progression of the SMAA positive cells to Col3.6 positive. SMAA green became evident by day 2 in the periosteum and there is an increase of strong SMAA associated with muscular blood vessels developing from the surrounding muscle (Fig 15A). From day 3 a number of examples of endothelial cells surrounded by SMAA positive cells with their elongated shape advancing toward the fracture site arising from the adjacent muscle or periosteal tissue (Figure 15B). These cells are either a weak green or are blue/green. An expansion of small muscular blood vessels with a strong SMAA signal also rapidly

Figure 15: Precallus phase of fracture repair.	
 Day 2 Fracture: G=SMA, B=Col3.6 **4** **3** **2** Figure 15A	 Day 3 Fracture: SMA=G; Col3.6=B Figure 15B.
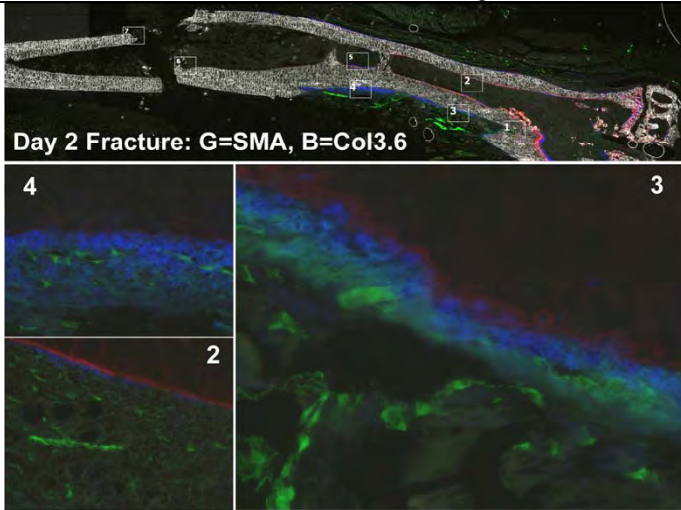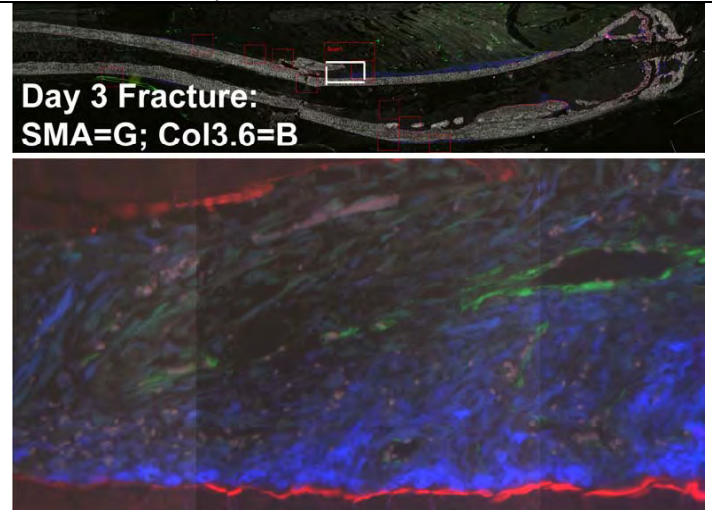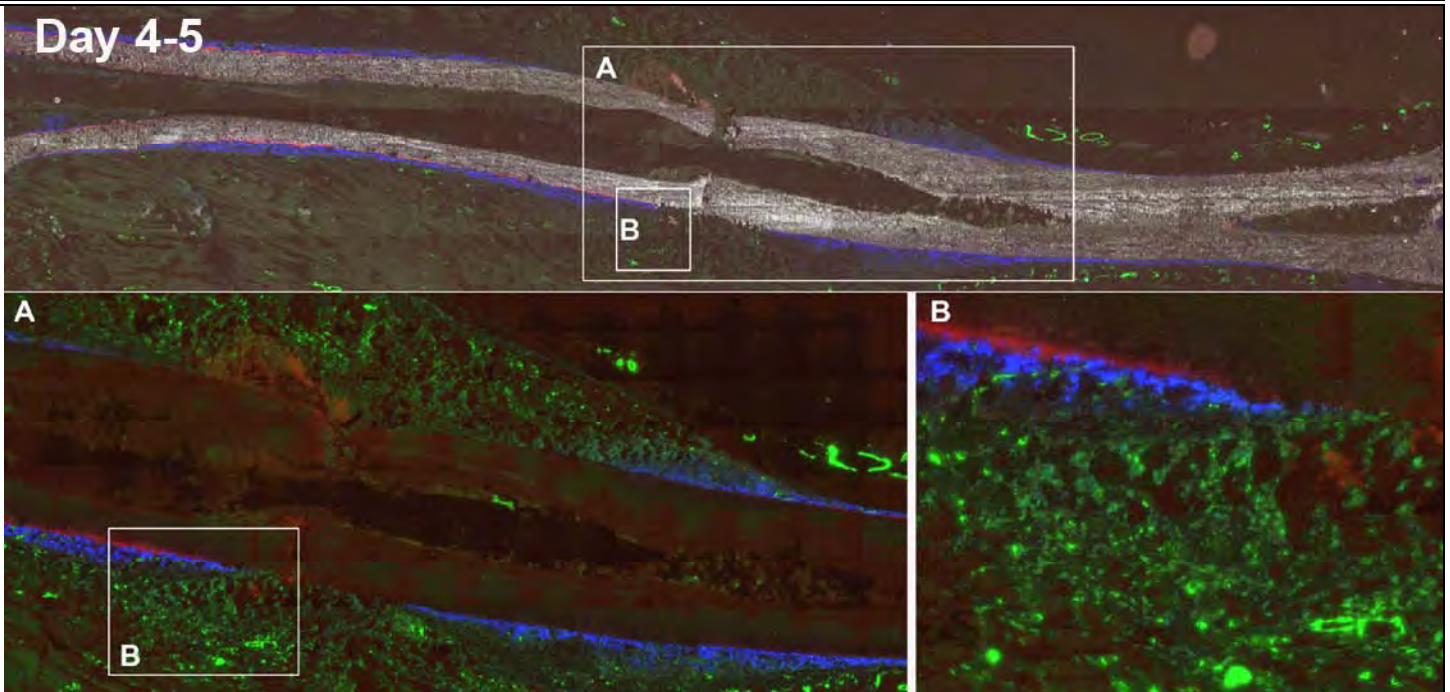
Figure 15C: Day 4-5. SMAA positive cells fill the zone that will become the fracture callus.
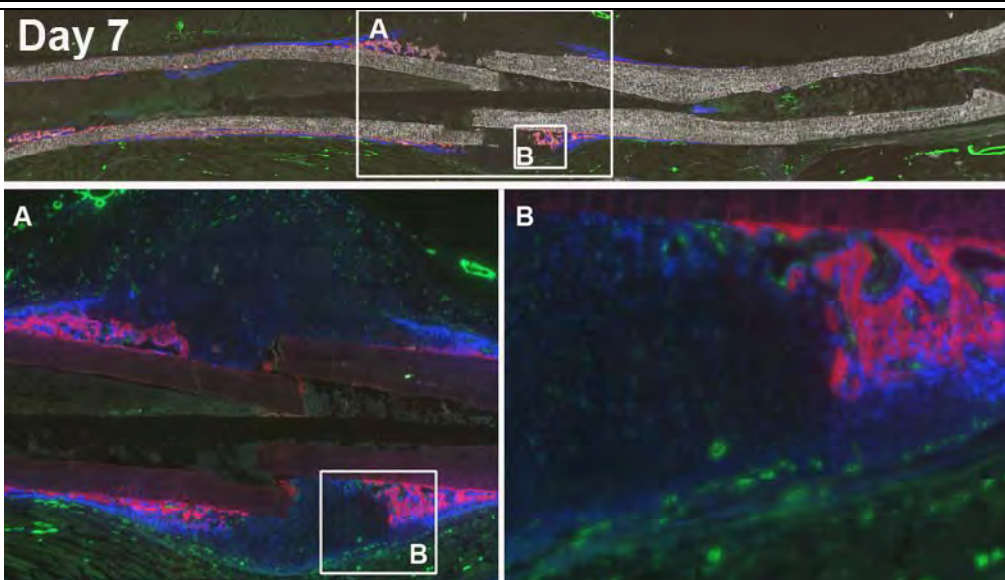
Figure 15D: Loss of the SMAA positive cells within the callus zone because they have begun to for chondrocytes. Some of the chondrocytes still have a faint green color suggesting that they have not completed the transition to a chondrocyte. The cells overlying the chondrocytes are entering the osteogenic lineage and are acquiring a blue/green appearance. Mineralized bone forms the base of the nascent callus.

develops 3-4 days post fracture further pointing to the importance of the vascular elements in this phase of the fracture repair.   By day 4-5, the SMAA positive cells have filled the zone over the fracture site (Figure 5C). Strong SMAA vessels are evident at the outer edge of the cellular accumulation. Col3.6blue cells with minimal mineralization form the base of the SMAA positive cells. By Day 7 the SMAA cells are no longer evident and are replaced with early cartilage cells. Scattered SMAA cells are still evident on the outer shell of the bridging element which is just beginning to become Col3.6 positive. Pending experiments using a endothelial reporter (Tie2), our working model of repair is endothelial ingrowth->pericyte/myofibroblast ingrowth and expansion->osteogenic differentiation. Strong SMAA expression during early fracture repair has been observed by others (7).

Osterix is thought to act as a late transcription factor for osteogenic differentiation. We obtained the Osterix-GFP reporter mice and crossed them with Col3.6blue. Figure 16 shows that Osx-green cells develop in the zone of cells that are yet to become Col3.6 positive. Agents that modify the magnitude and progression of this sequence of events will affect fracture repair (8). For example, intermittent PTH can be seen to exert its effect in the number of osterix GFP positive cells that develop during this phase of the repair process (not shown).
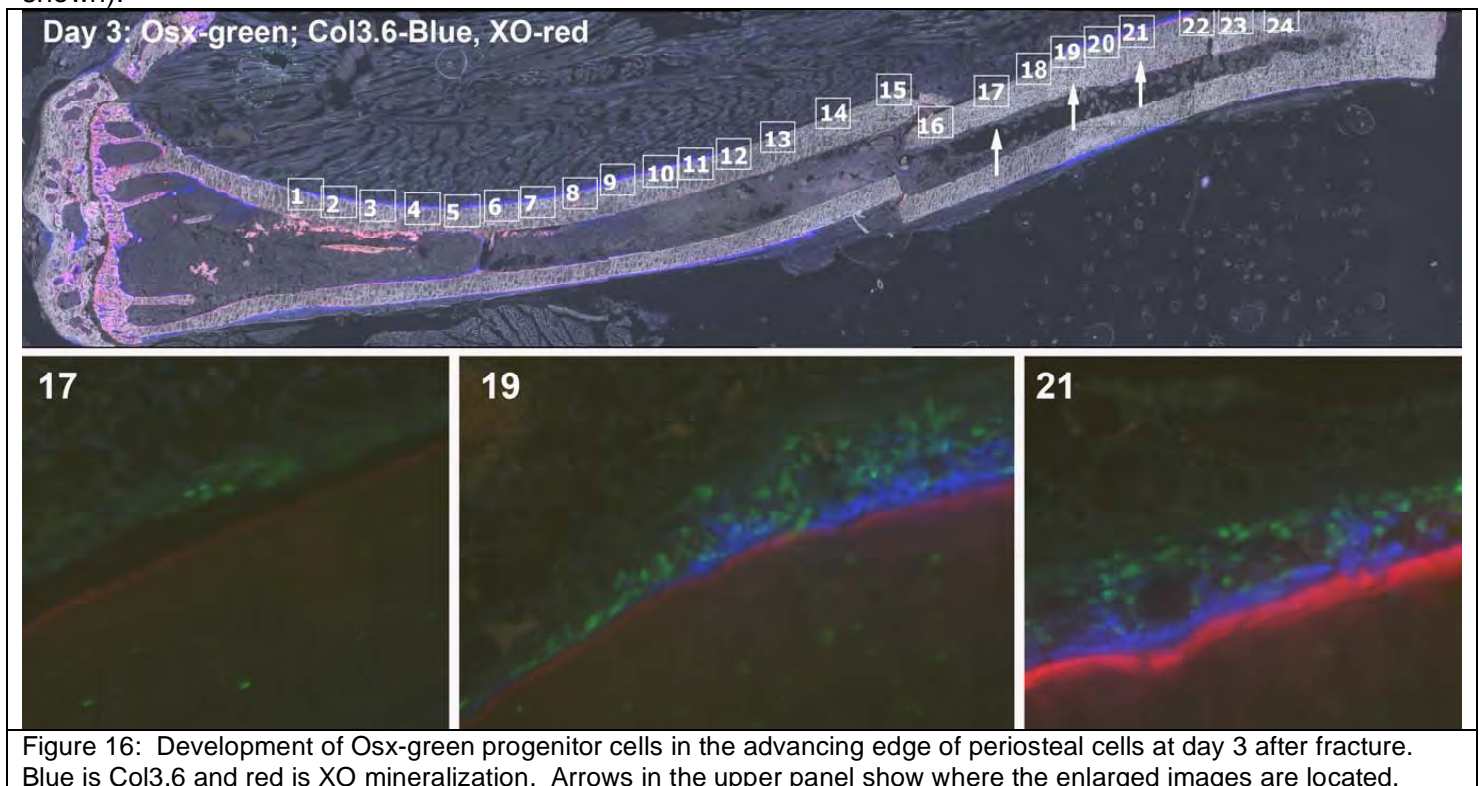

Figure 16: Development of Osx-green progenitor cells in the advancing edge of periosteal cells at day 3 after fracture. Blue is Col3.6 and red is XO mineralization. Arrows in the upper panel show where the enlarged images are located.

2. *Bridging and callus formation* – The obvious gradient of lineage progression of the earlier phase is less evident within the developing and resolving callus. While the outer shell of the callus is composed of Col3.6+ cells that progress to osteogenesis, the inner cells assume a chondrocytic appearance. Fractures were induced in mice that carried a Col2A1blue and Col3.6green reporter. We were surprised to observe the complexity of the chondrocytes (Figure 16) . Regions of blue cells, green cells, occasional blue/green cells and cells with no GFP activity were observed. Areas of mineralization surrounding Col2A1 only cells can be found. This pattern of reporter expression is not found in endochondral cartilage, but has been observed in fibrocartilage of the temporal mandibular joint. Work by other members of our group have demonstrated that the Col3.6+ chondrocytes express both type I and II collagen as well as BSP and aggrecan while the Col2A1 cells express type II but not type I collagen.

Thus the cartilage zone of the fracture is a complex cellular mixture of cells and the relationship of these cells to the stability of the callus and its subsequent resolution is yet to be understood. One gets the impression that the proliferating SMAA cells that initially expand into the base of the building callus differentiate into osteogenic lineage at sites where there is adequate endothelial support or into chondrocytes where vessels are lacking. If true, cartilage differentiation may reflect a relative failure of endothelial expansion. However the cartilage that does develop appears to be fibrocartilage in nature providing more mechanical stability than endochondral cartilage and thus contributing to the stabilization of the fracture zone.
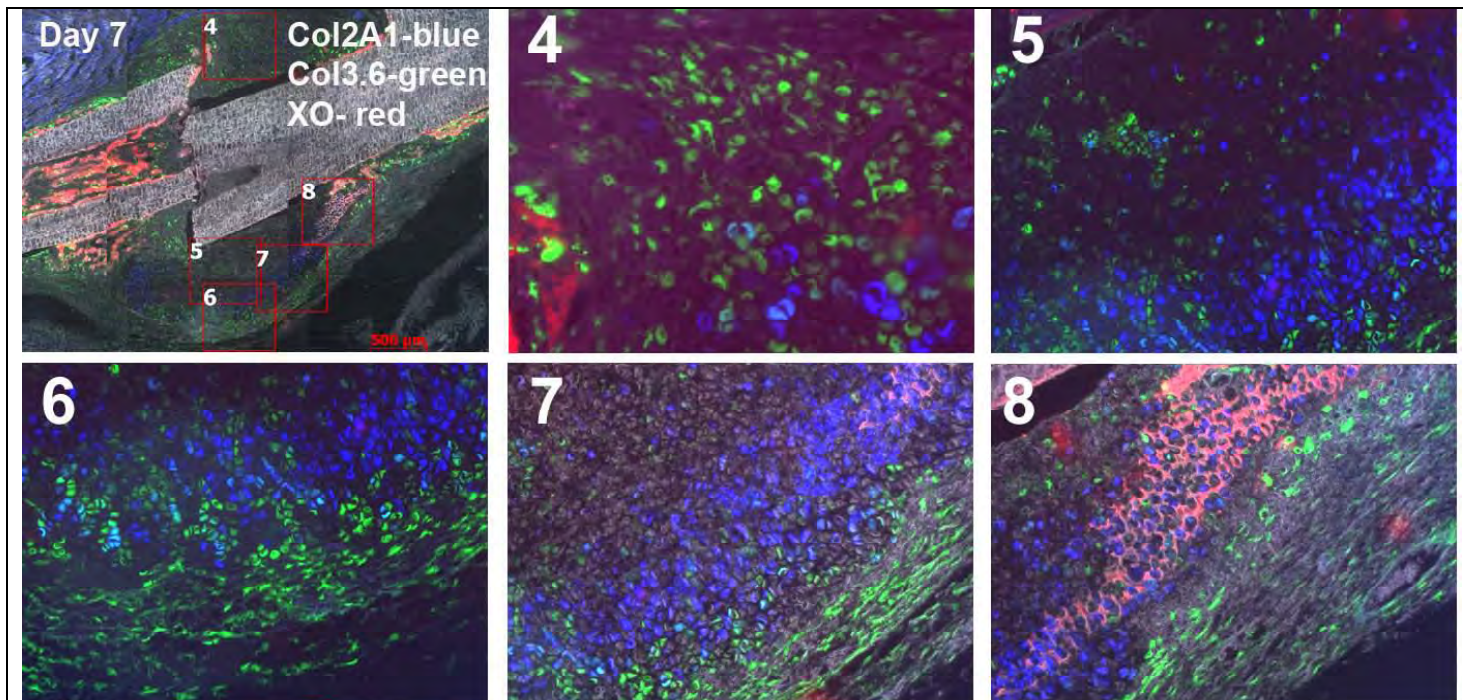
Figure 16: Fracture callus chondrocytes at day 7. Upper left panel localizes where the larger images are located.

3. *Callus resolution* – By two weeks after the fracture, the cartilage is being eroded by an advancing osteogenic front that is probably induced by hypertrophic cells and osteoclasts. The resulting woven bone is initially Col3.6+ which is rapidly changed to Col3.6/OC double positive and then OC only cells. We assume the cellular basis of remodeling and reintegrating the newly deposited bone into the existing bone is similar to the calvarial defect model and we have not investigated this process in the fracture until we understand it better in the defect model. Work by Dr. Ivo Kalajzic in our group has demonstrated dramatic differences in the microarray pattern of surface osteoblasts (Col2.3+) and matrix imbedded osteocytes (DMP+) and there is reason to believe that there is cellular heterogeneity within each of these populations. Developing reporters for these cells types and their relationship to the repair process will be required to understand what ultimately constitutes a successful repair. However that is not going to be an active area of investigation at this time.

B. Plans for the coming year

We will focus on the early events that precede callus formation with particular attention to the vascular elements and their relationship to skeletal progenitor expansion. Dr. Ushiku has mastered fluorescence-based in situ hybridization and its co-localization to the GFP image and this should provide new insights into what cells are making the essential growth factors for the early repair process. We also want to better understand the cellular organization of the cartilage core. Clearly there is a greater complexity than is revealed by a saffron-O histological section and the combination of the GFP reporters and in situ hybridization may provide clues to this process.

Objective 2B: Gain experience with the long bone segmental defect

At the time this grant was activated, Dr. Jay Lieberman assumed leadership of the Orthopedic Department at the University of Connecticut. He brought his research staff to our institution and thus we have in house surgical expertise for the long bone defect model (9, 10). Drs. Wang and Ushiku have participated in the surgical protocol using our GFP reporter mice in experiments performed to examine the effect of locally produced BMP2 on fracture repair. The reporter indicated that the majority of the osteoblasts that fill the defect come from surrounding bone, not the transduced cells that are implanted into the wound (Figure 17). In the coming year we will incorporate this model into our surgical repertoire. We will utilize the knowledge gained from the closed fracture model to understand the basis for non-union and begin to place the best scaffolds and progenitor cell mixtures to affect a closure.
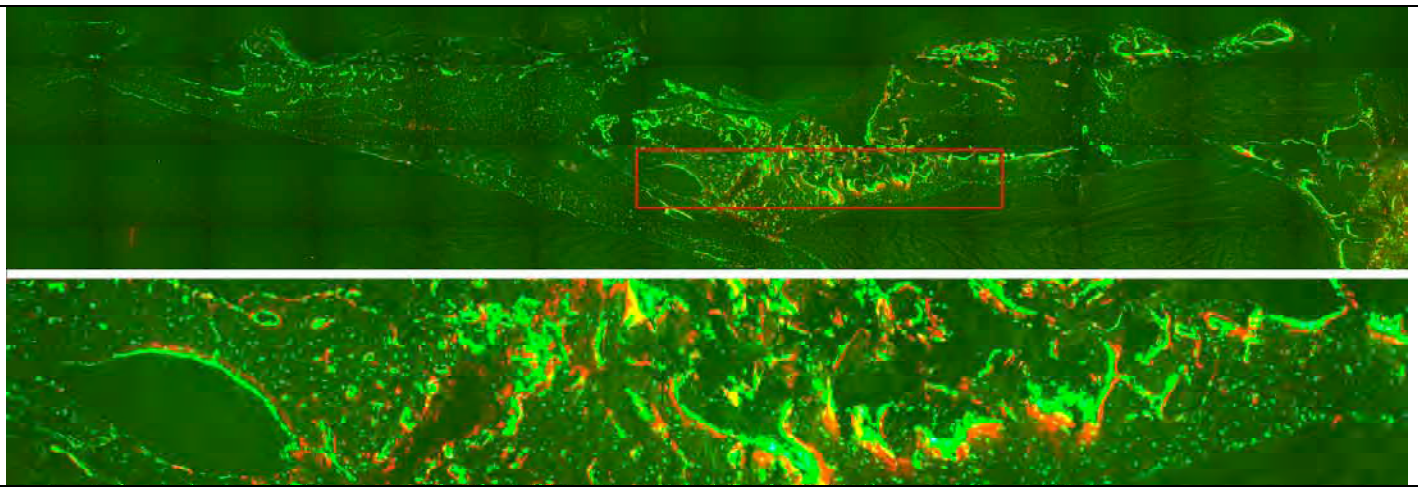
Figure 17: Repair of long bone lesion with BMP2 transduced bone marrow cells performed in a host mouse transgenic for the Col2.3GFP reporter. The donor cells were non-transgenic. The higher power image derived from the red boxed area shows strong GFP+ cells overlying the red XO mineralization line. The small GFP+ cells beneath the XO label are osteocytes. Thus the majority of the bone formed is host in origin because the reverse experiment (Col2.3 bone marrow into an non-transgenic host) did not generate GFP+ osteoblasts.

Objective 3A: Image analysis of repair lesions

A. Progress over the past year

Although the frozen histology that we have developed for preserving GFP expression in mineralized tissue does yield extremely colorful and informative images, its biggest advantage is the potential for quantitation so that comparisons are numeric rather than a subjective opinion. We initiated this project because a postdoctoral fellow trained in image analysis, Dr. Seung-Hyun Hong, joint the laboratory of Dr. Dong-Guk Shin in the Department of Computer Science at UCONN Storrs. Following the model that we developed for applying computer informatics to microarray data developed in my laboratory, we have a schedule in which Dr. Hong comes to Farmington once a week to scan sections that are prepared by our technical staff. The image files are transferred to Storrs to develop another aspect of the analysis. On Friday afternoon we hold our two-way videoconference with Storrs to review the progress and make plans for the coming week. Most of our efforts have focused on trabecular bone of the distal femur or vertebra so that we can compare our analysis with histomorphometric standards. We feel that the algorithms we develop for this region of bone will be applicable to bone formed in a repair zone.

1. Mineralized bone and mineralization lines can be imaged directly – The new tape transfer process does not fragment the mineralized portion of the bone (figure 18) and low autofluorescent backgound of the tape allows mineralization lines and GFP to imaged as discrete signals. Technically this step is performed on formalin fixed frozen blocks within two days after harvesting the tissue. Unlike plastic embedding and sectioning which can take 1-3 weeks to perform, our approach can generate images for analysis within a week after harvesting the sample.

Figure 18: Step for cutting cyrosections of non-decalcified bone. A segment of tape cut from sheet (A) to cover the embedded bone (B). The desired section is removed from the bone by the tape (C) and placed face down on the slide (D). The reproducibility of sections is illustrated in (E).

The section is recorded as a series of individual images that are stitched together to a higher degree of resolution than was provided by the commercial software provided by Zeiss. Each image is a stack of 3 or more separate exposures of light using DIC optics (mineralized tissue) and multiple fluorescent bands (e.g., blue, green, red and others). Figure 19 shows the superimposed DIC and green/blue mineralization lines of mice that were labeled with calcein and XO 7 and 2 days prior to sacrifice. The quality of the section and the distinct signals generated by the three exposures lend themselves to computer based image analysis.
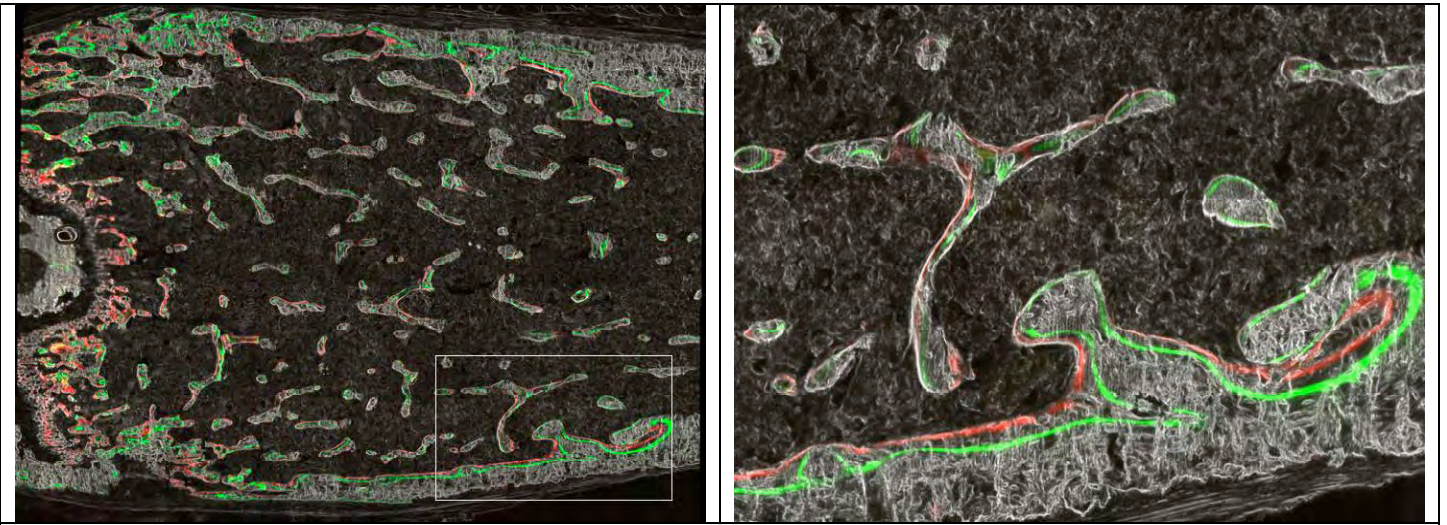
Figure 19: Our latest images using the low background tape transfer process. The distal femur of a non-transgenic mouse label 7 days apart by xylenol orange (XO) and calcein. The unfragmented and distinct separation of mineralized and fluorescent mineralization surfaces provides the localization landmarks to orient GFP cellular signals.

2. Computer algorthims for dynamic histomorphometric measurements compare favorably to manual measurements – Mice were double labeled and the same histological section were scored for traditional static and dynamic measurements using commercial products and manual tracing of bone surfaces and labeling lines. Likewise the computer algorithm thresholds for bone surface and related the single and double labeled surfaces back to the total bone surface. In addition the distance between the two labeling was recorded to acquire the bone matrix apposition rate. We have begun to validate our approach relative to manual methods and published reports.
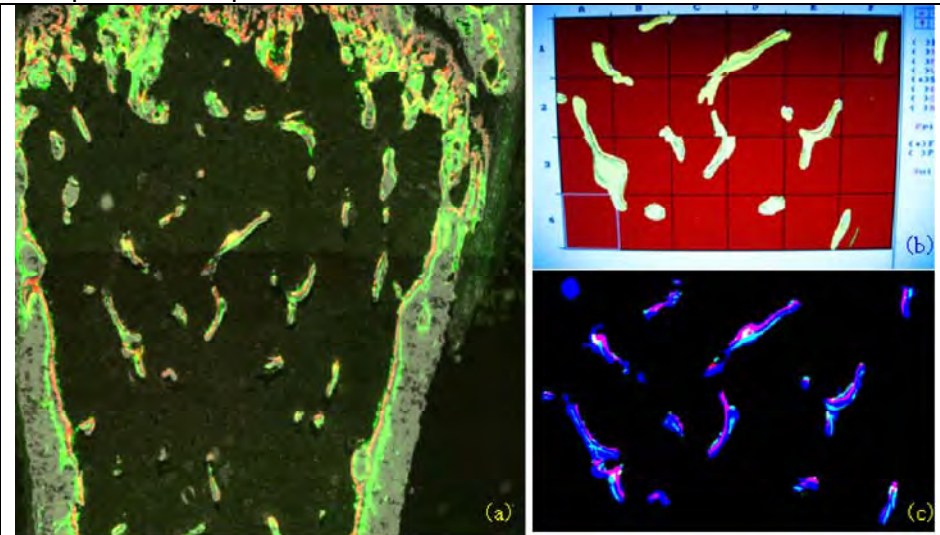

Figure 20: Comparison between the manual and computer generated histomorphometry. (a) DIC image showing the two mineralization labels. (b) screen shot of the image produced by the manual analysis. (c) segmented DIC image with mineralization labels produced by the automated method.

To demonstrate that the automatic approach is comparable to the manual approach or even better, we analyzed the same set of sections with both methods (Figure 20). For the manual analysis, we have relied on Dr. Boguslawa Koczon-Jaremko who was trained by the renowned bone histomorphometry expert Dr. Gloria Gronowicz of UCHC. Starting with the same image (Figure 20(a)), she independently carried out the analysis using the conventional method with OsteoMeasure (Figure 20(b)). Both approaches used same region of interest (ROI). Figure 20(c) is the outcome from the automatic segmentation. Table 1 shows the summary of comparing major indices (explained shortly in Section C.3 below) of two methods. There are slight variations, but more or less both results are very comparable.

Table 1.	sLS/BS(%)	dLS/BS(%)	GFP/BS(%)	Ir.L.Th(µm)	MAR(µm/day)	LS/BS(%)	BV/TV(%)
Manual	14.95	22.40	7.91	15.38	2.20	37.35	8.61
Automated	12.32	26.13	8.32	15.36	2.19	32.29	8.60

Our third attempt was to test whether our imaging and measurement protocols can reproduce some published results. We purchased 6 male and 6 female C57BL/6 mice and the same numbers of C3H male and female mice from Jackson Labs, and aged to 3.5 months and injected them with calcein 7 days and AC 2 days prior to sacrifice. Samples were processed for cryosectioning using the tape transfer step, and the unstained and non-decalcified sections were imaged by DIC, green and red fluorescence. The tiled distal femur was

selected for analysis using a computer-selected ROI that was 400 μm from the growth plate including about 1.215 mm^2. Figures 21(a) and 21(d) are, respectively, two example scanned images of C57BL/6 and C3H female mice. Figures 21(b) and 21(e) are computer selected ROIs. Figure 21(c) and 21(f) show the automated segmentation outcome of ROIs presented in pseudo colors.
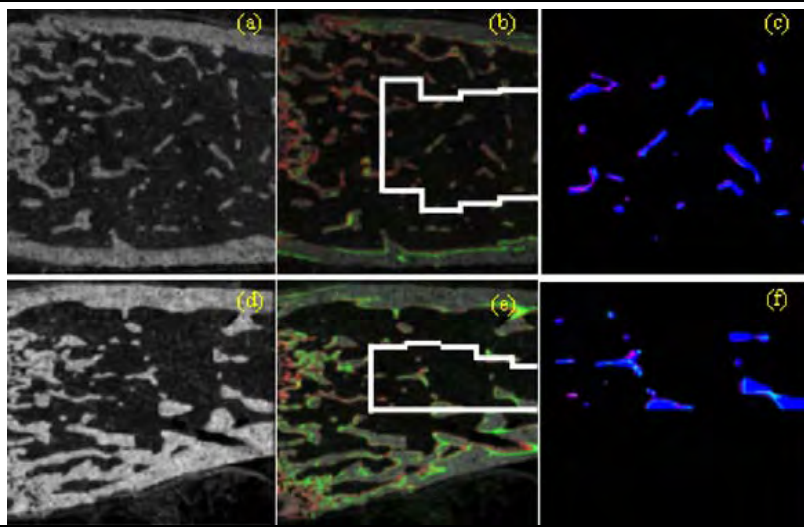

Figure 21: Analysis of dynamic histomorphometry of inbred mouse strains. Top row is C57Bl/6 while bottom row is C3H. (b, e) DIC images with mineralization lines; the solid lines are the computer selected region of interest. (c, f) Segmented trabeculae with labeling lines.

Table 2 shows the summary of primary measurements of a labeled surface relative to the total mineralized surface within the ROI. The analysis shows that the C57BL/6 females have a high bone formation rate but lower total bone volume relative to the males, while the C3H females have a marginally increased bone formation rate and equivalent total bone volume relative to males. When compared across the two lines of mice, there is an equivalent and higher BFR in the females and the difference in BFR across the two lines reflect the difference in males. These comparisons and others that can be made from the table is very similar to those that have been published using manual techniques (11-14) and gives us confidence that our thresholding and computational algorithms are reliable.

Table 2: Comparison of computer automated histomorphometry of distal femur of C57Bl/6 and C3H male and female mice.

C57Bl/6

		sLS/BS	dLS/BS	LS/BS	MS/BS	MAR(um)	BFR	BV/TV	Tb.Th
Female	1	30.31	11.74	42.05	26.90	1.17	31.58	3.45	19.63
	2	28.11	15.01	43.11	29.06	1.04	30.28	6.06	17.11
	3	28.23	4.65	32.88	18.77	1.20	22.53	3.52	17.72
	4	34.91	0.00	34.91	17.45	NaN2	NaN2	7.53	18.08
	5	34.59	23.12	57.71	40.42	1.12	45.43	8.58	18.50
	6	39.40	12.86	52.26	32.56	1.07	34.87	6.99	16.26
	mean	32.13	13.48	45.60	29.54	1.12	32.94	5.72	17.84
	std	4.84	6.65	9.64	7.92	0.07	8.32	2.23	1.29
Male	7	35.52	5.54	41.06	23.30	1.08	25.06	14.96	33.63
	8	28.07	8.53	36.60	22.57	0.73	16.57	12.09	22.02
	9	29.18	7.43	36.61	22.02	1.00	22.05	14.60	26.05
	10	26.83	8.20	35.02	21.61	0.92	19.83	13.35	24.12
	11	37.18	13.70	50.87	32.28	0.71	22.87	10.60	23.43
	12	25.35	8.49	33.84	21.16	1.00	21.26	7.64	18.96
	mean	30.35	8.65	39.00	23.82	0.91	21.27	12.21	24.70
	std	4.84	2.72	6.31	4.21	0.15	2.89	2.76	4.97
	mean	31.16	10.84	42.00	26.42	1.00	26.57	9.26	21.58
	std	4.68	5.26	8.30	6.55	0.16	8.30	4.16	5.09

C3H

		sLS/BS	dLS/BS	LS/BS	MS/BS	MAR(um)	BFR	BV/TV	Tb.Th
Female	1	33.82	17.98	51.81	34.90	0.87	30.36	10.77	19.92
	2	33.78	22.36	56.14	39.25	0.79	30.93	23.11	48.70
	3	31.46	14.42	45.87	30.14	1.36	40.85	14.60	29.15
	4	24.15	15.63	39.78	27.71	0.93	25.71	17.94	30.30
	5	27.21	18.25	45.46	31.86	0.98	31.22	9.63	28.53
	6	40.05	14.86	54.91	34.89	1.23	42.97	20.39	34.73
	mean	31.74	17.25	49.00	33.12	1.03	33.67	16.07	31.89
	std	5.58	2.97	6.34	4.09	0.22	6.72	5.36	9.54
Male	7	26.34	7.54	33.88	20.71	1.42	29.36	14.86	31.58
	8	41.46	12.09	53.55	32.82	0.74	24.26	15.77	33.78
	9	21.75	0.00	21.75	10.88	NaN2	NaN2	12.31	26.77
	10	31.69	15.22	46.90	31.06	1.22	37.93	23.81	49.48
	11	26.56	19.26	45.82	32.54	0.95	31.01	6.98	18.94
	12	27.37	12.12	39.49	25.80	0.85	21.89	13.60	27.34
	mean	30.68	13.25	43.93	28.59	1.04	28.89	15.00	32.23
	std	6.40	4.33	7.51	5.23	0.28	6.26	6.01	11.19
	mean	31.26	15.43	46.69	31.06	1.03	31.50	15.59	32.04
	std	5.68	4.04	7.05	4.99	0.24	6.67	5.40	9.78

t-test p-values							
B6 Female vs. B6 male	0.2804	0.0936	0.1160	0.0988	**0.0088**	**0.0160**	**0.0010**	**0.0092**
C3H Female vs. C3H male	0.3896	0.0620	0.1334	0.0776	0.4766	0.1270	0.3827	0.3795
B6 vs. Ch3	0.3819	**0.0168**	0.0845	**0.0387**	0.3775	0.0709	**0.0031**	**0.0033**

Abbreviations used are based on (15): sLS/BS - single labeled surface over bone surface; dLS/BS - double labeled surface over bone surface; LS/BS – labeled surface over bone surface which is the summation of double labeled surface and single labeled surface; MS/BS - mineralizing surface over bone surface and is calculated (dLS + sLS/2)/BS; MAR – mineral apposition rate is measured as the distance (μm) between the two mineralization lines divided by the interval between labeling; BFR - Bone formation rate is calculated as MAR×(MS/BS).

3. Computer based cellular histomorphometry provides additional measurements that are not possible with the manual method – Traditional histomorphometry that assesses the types of cell lining the bone surface utilize either paraffin or plastic embedded tissue, use of fluorescence based reporters is lost making computer thresholding difficult. The frozen histology maintains a fluorescent signal and we have exploited that feature. For example, when a green GFP reporter is incorporated into an experiment, its signal can be segregated distinct from a from a red mineralization line and the mineralized surface to permit the calculation of percent total surface or red-labeled surface covered by a green labeled osteoblasts. This feature will be applied to

studies designed to show an enrichment of bone progenitor cells relative to the starting material. Enriched cells carrying a blue label will be mixed with starting material carrying a green label prior to inoculating the scaffold. When bone is formed, the software will calculate the percentage of XO surface covered with blue or green osteoblasts. This type of experiments was performed on progenitors treated with PTH prior to inoculation and the result showed a modest increase (20%) in osteoblasts of the PTH treated cells.

Frozen sections have the additional advantage of preserving enzymatic and antigenic activity to a greater degree than other preservation methods. Thus after a section is imaged for its endogenous light and fluorescent signal, it can be processed for enzymatic or antigenic activity, re-imaged and aligned with the original image. The challenge is aligning the two images in a computer driven manner, particularly when the processing removes the mineralized portion of the slide. We think we have solved this problem by spotting a few fluorescent flow cytometry beads at opposite ends of the long bone specimen. The beads stick to the tape and act as an alignment anchor to register the second image with the first. This step has revealed that the processing of the sample causes a slight shrinkage of the tape but the computer software can compensate for this change to permit alignment back to the original image.

The alignment technique has been used to associate endogenous alkaline phosphatase (AP) and TRAP activity back to the original image. Both enzymatic stain protocols demineralize the sample. Our current protocol stains for AP first using red fluorescent substrate and is followed by a TRAP stain using a sapphire optimized substrate. The computer can distinguish these signals and calculate the percentage surface area of each cell type and whether it is associated with a XO labeled surface. We believe that this same technique will become useful when antibody and in situ stains for various growth factors are mapped back to specific cell types within a fracture or repair lesion.

B. Plans for the coming year

The algorithm developmental phase is complete and now the challenge is to implement and improve on the pipeline that will take the raw images from the database and return computed data. Dr. Shin has already developed a utility program that joints multiple data gathering, manipulation and inputs to existing applications for microarray data and this utility program (pipeline) will be modified for the image analysis application. Specific attention will be paid to the calvarial defect model with the intent to move it toward long bone defect as that model is developed.

Objective 3B: Archiving and retrieving histological imaging

A. Progress over the past year

As our reliance of histology as the primary data source has increased, the need for an organized and readily shared image retrieval system has become a major objective. No longer can images be stored on a personal hard drive using descriptive terms of meaning only to the individual who did the experiment. First we had to design the database and file management system and then convince the individuals performing the experiments to use it. Version 1 of the database system is now functional and getting users to incorporate this workflow is the current objective.

The program is called Image Manager. It organizes around a specific experiment. The experimental variables and the mice that are grouped into each experimental group are detailed. The histological sections that will be examined for each tissue from each mouse are also recorded. From this information a file structure is created on the local computer designed to hold the raw image files that will be generated by the microscope computer. Once the structure is correctly assembled it is transferred to the microscope computer and the central server. As the investigator records images from the histological sections, he/she places them into the appropriate folder utilizing an identifying file name that is assigned by the image manager program. At the end of the session, a linking button is activated which places the high resolution images on the server and creates a low resolution image of the file that is stored in the database. Once completed, the low-resolution images can be viewed via the server database by any computer and the high-resolution images can be down loaded for further processing.

It is through this file structure that we hope to develop a multidisciplinary communication mechanism in which additional data can be added to the initial files. For example in a repair experiment, photographs of the repair lesion, X-rays, µCT images, specialized stains, mechanical test results plus commentary fields can be deposited in an organized and retrievable manner to facilitate interaction particular in a videoconferencing context. As images are reviewed and critiqued, new experiments and interpretations are bound to evolve either during the meeting or subsequently when participants review the data as a single observer.

B. Plans for the coming year

We are still in the early working phase with this format for data interactivity and it is likely to evolve much differently as we gain more experience with it.

KEY RESEARCH ACCOMPLISHMENTS

A. Using the critical sized calvarial defect model
1. The host populates the defect with fibroblastic like cells that do not differentiate to osteoblasts.
2. Donor derived neonatal calvarial progenitor cells completely heal the defect by filling the gap with woven bone by 1 month and remodeling and integrating into host bone by 3-4 months.
3. Fresh marrow cell lack any osteogenic activity. They can contribute to the osteoclast population that is essential for donor derived bone remodeling.
4. Marrow adherent cells contain a low level of osteogenic activity. Enriching for the progenitors within this adherent population may be a viable source of clinically relevant progenitor cells.
5. The calvarial defect model is a rapid way to evaluate the osteogenic properties of various scaffold preparations.

B. Using GFP reporters in the long bone stabilized fracture model
1. Early progenitors develop 2-3 days post fracture at a significant distance from the fracture site. SMAA and osterix reporters label these cells.
2. A gradient of early to mature cells within the osteogenic lineage migrate toward the fracture site to form the bridging callus
3. The cartilage that forms resembles fibrocartilage more than endochondral cartilage.

C. Frozen fluorescent histology can produce high quality images amenable to computer based image analysis
1. Algorithms developed for dynamic histomorphometry of trabecular bone
2. The same image analysis programs will be applicable to bone repair models.

REPORTABLE OUTCOMES

1. Manuscripts, abstracts, presentations: Posters and oral presentations of this past year's work will be presented at the annual ASBMR meeting in Toronto. Manuscripts on the calvarial defect and closed fracture model are in the early writing stage.

> L. Wang, Y. Liu, P. Maye, D. W. Rowe. Use of GFP Reporter Mice for Assessing Osteoprogenitor Cell Activity in a Critical Size Calvarial Defect. Sa007.
>
> P. Maye, Y. Liu*, L. Wang*, M. Kronenberg*, D. Rowe. Dermo1 Lineage Tracing Identifies Early Osteoprogenitor Cells in Adult Murine Bone Marrow Mesenchymal Stem Cell Cultures, Sa051
>
> C. Ushiku, J. Xi, L. Wang, D. J. Adams1, D. W. Rowe. Use of GFP Reporters to Assess Cell Lineage in a Murine Model of Tibial Fracture Repair, M077.
>
> Y. H. Wang, L. Wang*, X. Jiang*, S. Hong*, D. W. Rowe. In Vivo Demonstration that PTH Acts on Early Osteoprogenitor Cells to Enhance Bone Formation During Repair of Critical-Size Calvarial Defects, M062.
>
> X. Jiang*, C. Ushiku*, H. Li*, D. W. Rowe. Dynamic Histomorphometry of Mineralized Tissue Using Cryosections of Murine Bone and Teeth, M138.

2. Training received: This award is supporting the postdoctoral research experience of a clinical orthopedic surgeon (Dr. Ushiku).

3. Development of new technologies and resources: The details of the frozen histology as applied to reparative lesions of bone is supported by this program. The animal model and GFP reporters will be shared with any investigative team.

4. Infomatics: The image analysis that is applied to bone histomorphometry and the database being developed to manage the imaging data are all a consequence of this program.

5. Funding applied for based on work supported by this award: Two SBIR applications have been submitted to develop the image analysis program to a commercial endeavor.

6. Employment or research opportunities: At the start of the project I had the opportunity to participate in the AFIRM review process followed by a tissue engineering workshop held by the FDA. Both venues underlined the issue of lack of communication between cell/developmental biologist and material scientists as they approach tissue engineering. I have tried to address this problem from the resources and new data arising from this award.
   a. Incorporation of Dr. Liisa Kuhn in this program – We have taught her research team how to work with GFP reporter mice and how to use our fluorescent microscopes to assess osteogenic differentiation for her in vitro studies of scaffolds materials. She in turn has acquired scaffold materials from outside

investigators to evaluate in our in vivo model. The activity will greatly expand next year.

   b. Dr. Mei Wei is a materials scientist at UConn Storrs has developed a series of scaffolds that are currently being evaluated in out calvarial defect model. This effort has lead to grant applications to NIH and NSF. An F33 grant was funded and it will support a sabbatical year in my laboratory beginning in September 2008. A BIRT application failed but a second round of funding has just been announced and we will respond.

   c. A small Connecticut medical device company, Doctors Research Group (DRG), produce a bone cement that is currently under FDA review. They have just funded a small contract to evaluate derivatives of this material as a scaffold for progenitor cells.

   d. DARPA announced a competition for a bone cement for long bone defect stabilization and healing. Because of the ongoing interactions with DRG and Dr. Wei, we responded to the announcement with a multi-team application that joined two material scientists at UCONN, two commercial materials groups, ourselves for the cell/tissue evaluation of these materials and Dr. Jay Lieberman for his expertise in the long bone defect model. Whether successful or not, the process of working across these scientific disciplines to assemble the application affirmed the importance of persisting in making this type of multidisciplinary interaction a part of everyday research life.

CONCLUSION

This award has allowed my laboratory to migrate its long-term interest in fundamental cell and molecular biology of the osteoblast lineage to a highly translational and practical application of cell based repair of a skeletal defect. It has lead us to develop new models and histological protocols to provide interpretable outcomes in a rapid and quantitative manner. We expect that the groundwork that was accomplished in the first year will be exploited in the remaining two years to clearly define the optimal scaffolds and clinically relevant cell preparations for skeletal repair. Looking forward to other opportunities that will be impacted by the current grant brings the focus to human cell based therapies. We are highly involved in the human embryonic stem cell and induced pluripotential cell research as a source for producing human bone progenitor cells. It is obvious that we will the need animal models to test this cell source and the scaffolds that are most supportive of their differentiation to mature osteoblasts. The models and technologies that have been worked out for a murine progenitor cell system will be readily adaptable to a humanized mouse model which we are currently in the process of developing. Over the next year or two we hope to be making this transition and we are very appreciative of the experience that the current funding has provided in the area of cell based skeletal repair.

REFERENCES:

1. Wang, L., Liu, Y., Kalajzic, Z., Jiang, X., and Rowe, D.W. 2005. Heterogeneity of engrafted bone-lining cells after systemic and local transplantation. *Blood* 106:3650-3657.

2. Boban, I., Jacquin, C., Prior, K., Barisic-Dujmovic, T., Maye, P., Clark, S.H., and Aguila, H.L. 2006. The 3.6 kb DNA fragment from the rat Col1a1 gene promoter drives the expression of genes in both osteoblast and osteoclast lineage cells. *Bone* 39:1302-1312.

3. Kalajzic, Z., Li, H., Wang, L.P., Jiang, X., Lamothe, K., Adams, D.J., Aguila, H.L., Rowe, D.W., and Kalajzic, I. 2008. Use of an alpha-smooth muscle actin GFP reporter to identify an osteoprogenitor population. *Bone* 43:501-510.

4. Dominici, M., Marino, R., Rasini, V., Spano, C., Paolucci, P., Conte, P., Hofmann, T.J., and Horwitz, E.M. 2008. Donor cell-derived osteopoiesis originates from a self-renewing stem cell with a limited regenerative contribution after transplantation. *Blood* 111:4386-4391.

5. Kumagai, K., Vasanji, A., Drazba, J.A., Butler, R.S., and Muschler, G.F. 2008. Circulating cells with osteogenic potential are physiologically mobilized into the fracture healing site in the parabiotic mice model. *J Orthop Res* 26:165-175.

6. McLain, R.F., Fleming, J.E., Boehm, C.A., and Muschler, G.F. 2005. Aspiration of osteoprogenitor cells for augmenting spinal fusion: comparison of progenitor cell concentrations from the vertebral body and iliac crest. *J Bone Joint Surg Am* 87:2655-2661.

7. Kinner, B., Gerstenfeld, L.C., Einhorn, T.A., and Spector, M. 2002. Expression of smooth muscle actin in connective tissue cells participating in fracture healing in a murine model. *Bone* 30:738-745.

8. Komatsubara, S., Mori, S., Mashiba, T., Nonaka, K., Seki, A., Akiyama, T., Miyamoto, K., Cao, Y., Manabe, T., and Norimatsu, H. 2005. Human parathyroid hormone (1-34) accelerates the fracture healing process of woven to lamellar bone replacement and new cortical shell formation in rat femora. *Bone* 36:678-687.

9. Gamradt, S.C., Abe, N., Bahamonde, M.E., Lee, Y.P., Nelson, S.D., Lyons, K.M., and Lieberman, J.R. 2006. Tracking expression of virally mediated BMP-2 in gene therapy for bone repair. *Clin Orthop Relat Res* 450:238-245.

10. Virk, M.S., Conduah, A., Park, S.H., Liu, N., Sugiyama, O., Cuomo, A., Kang, C., and Lieberman, J.R. 2008. Influence of short-term adenoviral vector and prolonged lentiviral vector mediated bone morphogenetic protein-2 expression on the quality of bone repair in a rat femoral defect model. *Bone* 42:921-931.

11. Sheng, M.H., Baylink, D.J., Beamer, W.G., Donahue, L.R., Rosen, C.J., Lau, K.H., and Wergedal, J.E., Histomorphometric studies show that bone formation and bone mineral apposition rates are greater in C3H/HeJ (high-density) than C57BL/6J (low-density) mice during growth. Bone 25:421-429, 1999.

12. Akhter, M.P., Iwaniec, U.T., Covey, M.A., Cullen, D.M., Kimmel, D.B., and Recker, R.R., Genetic variations in bone density, histomorphometry, and strength in mice. Calcif Tissue Int 67:337-344, 2000.

13. Klein, R.F., Shea, M., Gunness, M.E., Pelz, G.B., Belknap, J.K., and Orwoll, E.S., Phenotypic characterization of mice bred for high and low peak bone mass. J Bone Miner Res 16:63-71. 2001.

14. Sheng, M.H., Baylink, D.J., Beamer, W.G., Donahue, L.R., Lau, K.H., and Wergedal, J.E. Regulation of bone volume is different in the metaphyses of the femur and vertebra of C3H/HeJ and C57BL/6J mice. Bone 30:486-491, 2002.

15. Parfitt AM, Drezner MK, Glorieux FH, Kanis JA, Malluche H, Meunier PJ, Ott SM, and Recker RR, "Bone histomorphometry: standardization of nomenclature, symbols, and units. Report of the ASBMR Histomorphometry Nomenclature Committee," J Bone Miner Res 2:595-610, 1987.